Mon. Not. R. Astron. Soc. **387,** L28–L32 (2008) doi:10.1111/j.1745-3933.2008.00476.x

The L_X–M relation of clusters of galaxies

E. S. Rykoff,[1⋆†] A. E. Evrard,[2,3,4] T. A. McKay,[2,3,4] M. R. Becker,[2,5] D. E. Johnston,[6] B. P. Koester,[7,8] B. Nord,[2] E. Rozo,[9‡] E. S. Sheldon,[10] R. Stanek[3] and R. H. Wechsler[11]

[1]*Physics Department, University of California at Santa Barbara, 2233B Broida Hall, Santa Barbara, CA 93106, USA*
[2]*Physics Department, University of Michigan, Ann Arbor, MI 48109, USA*
[3]*Astronomy Department, University of Michigan, Ann Arbor, MI 48109, USA*
[4]*Michigan Centre for Theoretical Physics, Ann Arbor, MI 48109, USA*
[5]*Department of Physics, The University of Chicago, Chicago, IL 60637, USA*
[6]*Jet Propulsion Laboratory, 4800 Oak Grove Drive, Pasadena, CA 91109, USA*
[7]*Department of Astronomy and Astrophysics, The University of Chicago, Chicago, IL 60637, USA*
[8]*Kavli Institute for Cosmological Physics, The University of Chicago, Chicago, IL 60637, USA*
[9]*The Ohio State University, Columbus, OH 43210, USA*
[10]*Centre for Cosmology and Particle Physics, Physics Department, New York University, New York, NY 10003, USA*
[11]*KIPAC, Physics Dept. and SLAC, Stanford University, Stanford, CA 94305, USA*

Accepted 2008 March 24. Received 2008 March 24; in original form 2008 February 7

ABSTRACT

We present a new measurement of the scaling relation between X-ray luminosity and total mass for 17 000 galaxy clusters in the maxBCG cluster sample. Stacking subsamples within fixed ranges of optical richness, N_{200}, we measure the mean 0.1–2.4 keV X-ray luminosity, $\langle L_X \rangle$, from the *ROSAT* All-Sky Survey. The mean mass, $\langle M_{200} \rangle$, is measured from weak gravitational lensing of SDSS background galaxies. For $9 \leqslant N_{200} < 200$, the data are well fitted by a power law, $\langle L_X \rangle / 10^{42}\, h^{-2}\, \mathrm{erg\,s^{-1}} = [12.6^{+1.4}_{-1.3}\,(\mathrm{stat}) \pm 1.6\,(\mathrm{sys})](\langle M_{200} \rangle / 10^{14}\, h^{-1}\, \mathrm{M}_\odot)^{1.65\pm0.13}$. The slope agrees to within 10 per cent with previous estimates based on X-ray selected catalogues, implying that the covariance in L_X and N_{200} at a fixed halo mass is not large. The luminosity intercept is 30 per cent, or 2σ, lower than that determined from the X-ray flux-limited sample of Reiprich & Böhringer, assuming hydrostatic equilibrium. This slight difference could arise from a combination of Malmquist bias and/or systematic error in hydrostatic mass estimates, both of which are expected. The intercept agrees with that derived by Stanek et al. using a model for the statistical correspondence between clusters and haloes in a *WMAP3* cosmology with power spectrum normalization $\sigma_8 = 0.85$. Similar exercises applied to future data sets will allow constraints on the covariance among optical and hot gas properties of clusters at a fixed mass.

Key words: galaxies: clusters: general – X-rays: galaxies: clusters.

1 INTRODUCTION

Bulk properties of galaxy clusters, such as galaxy richness and velocity dispersion, X-ray temperature and luminosity, mean weak gravitational lensing shear and X-ray hydrostatic mass display strong internal correlations (for reviews, see Rosati, Borgani & Norman 2002; Voit 2005). Although these correlations are anticipated by dimensional arguments – the 'bigger things are bigger in all measures' perspective – detailed theoretical expectations are complicated by baryon evolution uncertainties. Even with some baryon model prescribed, the stochastic nature of the halo evolution in a hierarchical clustering framework will impose variance about the mean behaviour, the scale of which is likely to be sensitive to the baryon prescription.

Improved understanding of cluster scaling relations is desirable on both astrophysical and cosmological grounds. Better astrophysical models of galaxy and hot gas evolution in haloes will improve constraints on cosmological parameters obtained from studies of cluster samples (e.g. Vikhlinin et al. 2006; Mantz et al. 2007; Rozo et al. 2007).

The relation between X-ray luminosity L_X and halo mass M is a diagnostic of the halo baryon fraction and the entropy structure of the intracluster gas. From X-ray data alone, constraints on the L_X–M relation have been obtained using either direct or statistical arguments. The direct approach assumes that the intracluster gas is

⋆E-mail: erykoff@physics.ucsb.edu
†TABASGO Fellow.
‡CCAPP Fellow.

in hydrostatic equilibrium, so that observations of the X-ray surface brightness, which provides L_X, and the X-ray temperature profile can be combined to estimate thermal pressure gradients and, hence, cluster binding masses. Reiprich & Böhringer (2002, hereafter RB02) measured the L_X–M relation in this manner for the X-ray flux-limited HIFLUGCS sample of roughly 100 clusters (Finoguenov, Reiprich & Böhringer 2001). The statistical approach, on the other hand, assumes a form for the likelihood, $P(L_X|M, z)$, which is convolved with the space density of haloes in a given cosmology to predict cluster counts as a function of X-ray flux and redshift. This approach was applied by Stanek et al. (2006, hereafter S06) to the flux-limited REFLEX survey (Böhringer et al. 2004) using halo space densities calibrated for a Λ cold dark matter (ΛCDM) cosmology (Jenkins et al. 2001; Evrard et al. 2002).

A third approach to the L_X–M relation employs weak gravitational lensing mass estimates derived from shear patterns of background galaxies in deep optical imaging of cluster fields. Recently, Bardeau et al. (2007) and Hoekstra (2007) have performed such analysis of 11 and 20 clusters, respectively, at redshifts near $z \sim 0.25$. These studies provide a powerful cross-check between the two methods, but provide a weaker constraint on the mass scaling as they focus on the X-ray luminous tail of the cluster population.

In this Letter, we extend the dynamic range of the third approach using a large, uniform sample. We present the L_X–M relation derived from ∼17 000 optically selected galaxy clusters in the maxBCG catalogue (Koester et al. 2007b). Binning clusters by optical richness, N_{200}, we measure the mean X-ray luminosity, $\bar{L}_X \equiv \langle L_X|N_{200}\rangle$, using data from the *ROSAT* All-Sky Survey (RASS: Voges et al. 1999). Details of the method are described in Rykoff et al. (2008, hereafter R08). The mean mass, $\bar{M}_{200} \equiv \langle M_{200}|N_{200}\rangle$[1] of each bin is measured from an analysis of the stacked weak gravitational lensing signal from SDSS galaxy images. Measurements of the shear are presented in Sheldon et al. (2007), and masses are derived by Johnston et al. (2007).

We begin with a brief description of the input data and the methods. We then present measurements of $\bar{L}_X$ and $\bar{M}_{200}$ for richness-binned maxBCG clusters, and compare the resultant scaling relation to the relations found by applying direct or statistical arguments to X-ray flux-limited samples. Throughout this Letter, we assume a flat, ΛCDM cosmology with $H_0 = 100\,h\,\mathrm{km\,s^{-1}}$ and $\Omega_m = 1 - \Omega_\Lambda = 0.3$. In addition, our measurements are quoted at $z = 0.25$, close to the median redshift of the cluster catalogue. Following R08, the X-ray luminosities are measured in the 0.1–2.4 keV observer frame, and k-corrected to rest-frame 0.1–2.4 keV at $z = 0.25$.

2 INPUT DATA

Input data for this study come from two large-area surveys: the Sloan Digital Sky Survey (SDSS: York et al. 2000) and RASS. SDSS imaging data are used to select the clusters and to measure the weak lensing shear around their centres. RASS data provide 0.1–2.4 keV X-ray luminosities, L_X, measured within r_{200}. Here, we briefly describe the maxBCG cluster catalogue, binning strategies, and our methods for calculating mean mass and X-ray luminosity.

[1] Here, M_{200} is the mass within a sphere of radius r_{200} that encompasses a mean density of 200 $\rho_c(z)$, with ρ_c the critical density.

Table 1. $\langle L_X|N_{200}\rangle$ and $\langle M_{200}|N_{200}\rangle$.

N_{200} range	r_{200} (h^{-1} Mpc)	$\bar{L}_X$ (0.1–2.4 keV) ($10^{42}\,h^{-2}\,\mathrm{erg\,s^{-1}}$)	$\bar{M}_{200}$ ($10^{14}\,h^{-1}\,M_\odot$)
9–11	0.49	2.72 ± 0.35	0.441 ± 0.080
12–17	0.55	5.65 ± 0.37	0.600 ± 0.085
18–25	0.64	12.8 ± 0.98	0.96 ± 0.13
26–40	0.77	30.6 ± 2.3	1.68 ± 0.23
41–70	0.90	56.7 ± 4.5	2.52 ± 0.36
71–188	1.20	209 ± 31	5.69 ± 0.88

2.1 maxBCG catalogue

The maxBCG cluster catalogue provides sky locations, redshift estimates, and richness values for the cluster sample we employ. Details of the selection algorithm and catalogue properties are published elsewhere (Koester et al. 2007a,b). In brief, maxBCG selection relies on the observation that the galaxy population of rich clusters is dominated by bright, red galaxies clustered tightly in colour (the E/S0 ridgeline). Since these galaxies have old, passively evolving stellar populations, their $g - r$ colour closely reflects their redshift. The brightest such red galaxy, typically located at the peak of galaxy density, defines the cluster centre.

The maxBCG catalogue is approximately volume-limited in the redshift range $0.1 \leqslant z \leqslant 0.3$, with very accurate photometric redshifts ($\delta z \sim 0.01$). Studies of the maxBCG algorithm applied to mock SDSS catalogues indicate that the completeness and purity are very high, above 90 per cent (Koester et al. 2007b; Rozo et al. 2007). The maxBCG catalogue has been used to investigate the scaling of galaxy velocity dispersion with cluster richness (Becker et al. 2007) and to derive constraints on the power spectrum normalization, σ_8, from cluster number counts (Rozo et al. 2007).

The primary richness estimator used here is N_{200}, defined as the number of E/S0 ridgeline cluster members brighter than $0.4L_*$ (in i band) found within $r_{200}^{\mathcal{N}}$ of the cluster centre (Hansen et al. 2005). An analysis of the mean weak lensing profiles of the clusters stacked in bins of N_{200} (Johnston et al. 2007, and Section 2.3) provides an improved measure of the scaled apertures, r_{200}. These radii are smaller, by ∼50 per cent on average, than $r_{200}^{\mathcal{N}}$. Our mass and luminosity estimates in this Letter consistently employ r_{200} derived from the weak lensing profiles. However, we remain consistent with the original catalogue's richness parameter, N_{200}, defined within the larger $r_{200}^{\mathcal{N}}$ radius.

As a cross-check, we also bin the sample using a secondary richness estimator, L_{200}, the total k-corrected i-band luminosity of the cluster members. The order parameters, N_{200} and L_{200}, are strongly correlated, especially for the richest clusters. We use six richness bins with $N_{200} \geqslant 9$, described in Table 1, based on those used in the weak lensing analysis of Sheldon et al. (2007). The total number of clusters is 17 335.

2.2 Measuring $\bar{L}_X$

We measure the mean 0.1–2.4 keV X-ray luminosity, $\bar{L}_X$, of the clusters in each bin by stacking photons from RASS. The typical RASS exposure time for maxBCG clusters is ∼400 s, too short to allow significant detections for all but the brightest individual clusters. By binning on N_{200} or L_{200} we can take advantage of the large number of maxBCG clusters. The stacking method is described in detail in R08, but there are a few differences in the analysis for this Letter which we highlight here.

We stack all the photons in a scaled aperture from clusters in a given richness or optical luminosity bin, treating the brightest cluster galaxy selected by the maxBCG algorithm as the centre of each cluster. In R08, we show that this assumption for centring does not introduce a significant bias in the calculation of $\bar{L}_X$. For consistency with the cluster mass calculations in Johnston et al. (2007), we scale all radii and luminosities to $z = 0.25$. This scale redshift is slightly larger than that used in R08, but does not significantly change $\bar{L}_X$. After building scaled photon maps, we construct images, radial profiles, and spectra, and calculate an unabsorbed, rest-frame mean luminosity, $\bar{L}_X$, for each bin. The X-ray luminosities are measured within scaled apertures, r_{200}. These radii are smaller than those used in the analysis of R08. However, as L_X is proportional to the gas density squared, most of the flux originates near the dense core and the effect of this re-scaling is modest, reducing the measured values of $\bar{L}_X$ by ∼10–15 per cent.

The best-fitting spectral temperatures are used to k-correct the observed 0.1–2.4 keV emission to the rest frame at $z = 0.25$. Values for the case of N_{200} binning are listed in Table 1. As shown in R08, the data are well fitted by a power-law form

$$\langle L_X|N_{200}\rangle = (42.1 \pm 1.7)\,(N_{200}/40)^{1.88\pm0.06} \times 10^{42}\,\mathrm{erg\,s^{-1}}. \quad (1)$$

2.3 Measuring $\bar{M}_{200}$

The mean projected surface density contrast, measured from the shear of faint background galaxies as a function of projected distance from the cluster centre, was calculated by Sheldon et al. (2007) for the binned samples employed in this Letter. However, as maxBCG clusters are not guaranteed to be centred on the mass density peaks of dark haloes, Johnston et al. (2007) calculate mean cluster masses using a mass model that incorporates a degree of halo miscentring.

Specifically, the projected surface density contrast in a given bin is modelled as a sum of four components: (i) a small-scale component from the stellar mass of the central galaxy; (ii) a mean NFW (Navarro, Frenk & White 1997) halo; (iii) a large-scale component arising from the clustering of haloes (the two-halo term); and (iv) a correction for the subset of clusters with BCG centres offset from halo centres. The mean halo mass, $\bar{M}_{200}$, and its uncertainty are obtained by marginalizing over the posterior probability distribution using a Markov Chain Monte Carlo (MCMC) method. The resultant masses, listed in Table 1, scale as a power law in richness:

$$\langle M_{200}|N_{200}\rangle = (2.1 \pm 0.3)\,(N_{200}/40)^{1.28\pm0.04} \times 10^{14}\,\mathrm{M_\odot}, \quad (2)$$

where the error in the intercept is dominated by systematic uncertainties in the photometric redshifts of background galaxies, in the absolute shear calibration, and in the calibration of the miscentring model.

3 THE $\bar{L}_X$–$\bar{M}_{200}$ RELATION

In Fig. 1, we plot the mean luminosities and lensing masses using binning in N_{200} (filled symbols; Table 1) or in L_{200} (open symbols). The two binning choices offer consistent results. The grey band shows the best-fitting maxBCG–RASS relation ($\pm\,1\sigma$) from N_{200} binning:

$$\langle L_X|N_{200}\rangle = 12.6^{+1.4}_{-1.3}\left(\frac{\langle M_{200}|N_{200}\rangle}{10^{14}\,h^{-1}\,\mathrm{M_\odot}}\right)^{1.65\pm0.13} 10^{42}\,\mathrm{erg\,s^{-1}}. \quad (3)$$

We estimate an additional systematic error of ±1.6 in normalization due to the mass scale uncertainties described in the previous section. The two additional lines show results from X-ray flux-limited cluster samples. The dashed line shows the results from the HIFLUGCS clusters of RB02 using hydrostatic mass estimates. The data have been re-fitted by S06 after converting their luminosity and mass estimates to ΛCDM cosmology (see section 3.4 in S06). The dot–dashed line is the X-ray count-matching result of S06 for a ΛCDM model with $\Omega_m = 0.24$, spectral index $n_s = 1$, and power spectrum

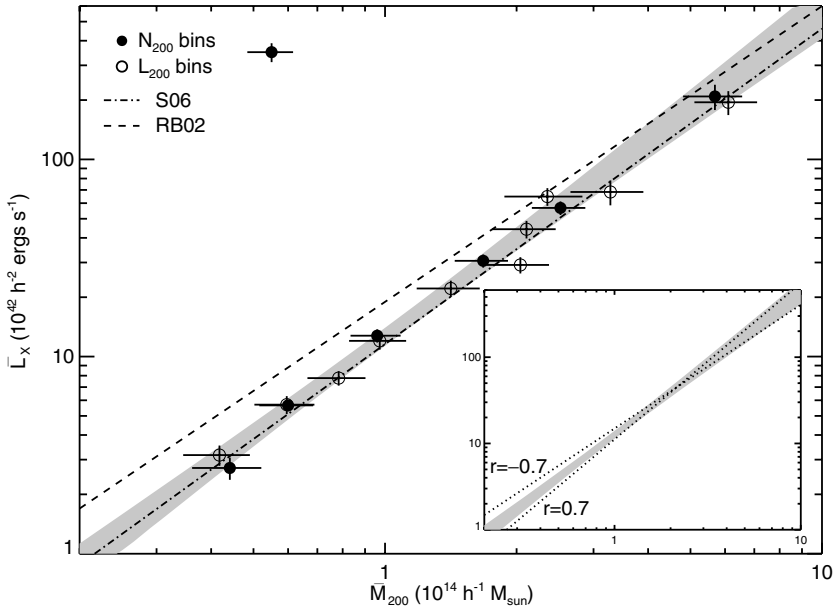

Figure 1. Points show maxBCG–RASS (algebraic) mean L_X and M_{200} values found by binning on N_{200} (solid circles) or L_{200} (empty circles). The dark grey band represents the $\pm1\sigma$ contours on the best-fitting relation using the N_{200} bins. The dot-dashed line shows the S06 relation, while the dashed line shows the S06 fit to the HIFLUGCS clusters from RB02 based on hydrostatic masses. Both relations have been scaled assuming self-similar evolution (see Section 3). The error bar in the legend shows the typical 1σ systematic error in the SDSS lensing masses, representing an overall shift in normalization that is possible in the maxBCG–RASS relation. The inset plot indicates the effects on the slope due to covariance between L_X and N_{200} at a fixed mass (r), as described in Section 4. If L_X and N_{200} at a fixed mass are correlated ($r = 0.7$), this will bias the slope steeper, and if they are anticorrelated, this will bias the slope shallower.

normalization $\sigma_8 = 0.85$; the inferred scatter in L_X at a fixed mass is $\sigma_{\ln L|M} = 0.40$. Both the RB02 and S06 results are quoted at the median redshift of the maxBCG cluster sample, $z = 0.25$, by assuming self-similar evolution, $L \sim \rho_c^{7/6}(z)$. This raises the L_X normalization of each by 27 per cent. Finally, to properly compare with the algebraic mean luminosity of maxBCG–RASS, we adjust the normalizations of RB02 and S06 by a factor $\exp(0.5\sigma^2_{\ln L|M})$, resulting in an ∼8 per cent increase in luminosity at a fixed mass.

The slope of the maxBCG–RASS relation, 1.65 ± 0.13, agrees well with the values found previously. The RB02 result, 1.50 ± 0.08, is somewhat shallower, but not significantly so, and the S06 result, 1.59 ± 0.05, is consistent with the present determination. The normalization of the maxBCG–RASS relation is consistent with the S06 results, with the RB02 masses lying 2σ low. Further discussion of these results is in Section 4 below.

The maxBCG–RASS normalization can be compared with recent lensing results published for small samples of massive clusters at $z \sim 0.25$. Bardeau et al. (2007) and Hoekstra (2007) performed weak lensing analyses of 11 and 20, respectively, individual clusters. Both studies focus on selected high-luminosity clusters, with $L_X > 10^{44}\ h^{-2}\,\mathrm{erg\,s^{-1}}$, at redshifts near the median of the maxBCG catalogue. Both papers find a correlation between L_X and M_{200}, but with noisy lensing mass estimates. As each study employs a different convention for L_X, we have recalculated L_X for these clusters using RASS photon data (see section 4.1 in R08). Fixing the slope at 1.6, we compute the normalization of $L_X/10^{44}\ h^{-2}\,\mathrm{erg\,s^{-1}}$ at $10^{15}\ h^{-1}\,\mathrm{M}_\odot$, finding 11 ± 2 and 5.0 ± 0.6 for the Bardeau et al. (2007) and Hoekstra (2007) clusters, respectively. At this high mass scale, the Hoekstra (2007) normalization is consistent with our value, while the Bardeau et al. (2007) is $\sim 2\sigma$ larger. A full accounting for this discrepancy is beyond the scope of this work.

4 DISCUSSION

The good level of agreement displayed in Fig. 1 among three independent approaches to determining the L_X–M relation indicates that optical and X-ray selection methods are finding similar populations of massive haloes. Furthermore, the maxBCG–RASS result extends to a lower mass scale than is probed by RB02 and S06. In this section, we point out effects that could lead to differences among the three measurements. The discussion is aimed at raising issues to be addressed by more detailed analysis in future work.

Non-zero bias in hydrostatic mass estimates, displayed in early, low-resolution gas simulations (Evrard 1990), is a possible source of systematic error that would shift the RB02 result relative to the true relation. Recent studies using mock X-ray exposures of numerical simulations predict a systematic underestimate of binding mass at the level of -0.25 in $\ln M$ (Rasia et al. 2005; Nagai, Vikhlinin & Kravtsov 2007). Correcting the RB02 result by this amount would more closely align it with the maxBCG–RASS relation. Assuming that the latter is an unbiased estimate of the underlying halo relation, the luminosity offset between the two relations measures the Malmquist bias arising from the X-ray flux limit of the HIFLUGCS sample used by RB02. Good agreement would signal a small bias, meaning small intrinsic scatter ($\lesssim 10$ per cent) between luminosity and mass. Such small scatter is considered unlikely by the analysis of S06.

A separate argument can be made based on slope estimates. If hydrostatic mass estimates scale with true mass as $\langle M_{\rm est}\rangle \propto M_{\rm true}^{1+\epsilon}$, then one would expect the RB02 slope to differ by 1.5ϵ from the maxBCG–RASS value. The measured slope difference, 0.15 ± 0.15, implies $\epsilon = 0.1 \pm 0.1$. Strongly mass-dependent hydrostatic biases are therefore ruled out.

One could shift the RB02 result to higher masses without requiring a major reduction in scatter, $\sigma_{\ln M|L}$, as constrained in S06. This would require shifting the S06 result by modifying the assumed cosmology. The luminosity normalization is sensitive to power spectrum normalization, $L_X \sim \sigma_8^{-4}$, so raising σ_8 to 0.95 would shift the S06 result to lower L_X and preserve the current level of Malmquist bias for the RB02 result. However, this adjustment would offset the S06 and maxBCG–RASS relations at the 2σ level.

Since it is binned by richness, the maxBCG–RASS result is sensitive to covariance among L_X and N_{200} at fixed M_{200}. Simulations suggest mild anticorrelation, as at a fixed mass high-concentration haloes have higher L_X but fewer galaxies (Wechsler et al. 2006). As an illustration of the effect of covariance, consider the case of a bivariate, lognormal distribution for L_X and N_{200} with constant covariance. The off-diagonal term can be characterized by the correlation coefficient, $r \equiv \langle \delta_{\ln L}\delta_{\ln N}\rangle$, where $\delta_{\ln X} = (\ln X - \ln \bar{X})/\sigma_{\ln X}$ are the normalized deviations from the mean relation.

Consider a mass function that is a local power law, $\mathrm{d}n/\mathrm{d}\ln M \sim M^{-\alpha} = \mathrm{e}^{-\alpha\mu}$, where $\mu \equiv \ln M$. Convolving this function with the bivariate lognormal, and using Bayes' theorem allows one to write the conditional likelihood $P(\ell,\ \mu \mid \nu)$, where $\ell \equiv \ln L_X$ and $\nu \equiv \ln N_{200}$. The result is a bivariate Gaussian with mean mass $\bar{\mu}(\nu) = \bar{\mu}_0(\nu) - \alpha\sigma^2_{\mu|\nu}$, with $\bar{\mu}_0(\nu)$ the inverse of the input mean richness–mass relation and $\sigma_{\mu|\nu}$ the scatter in mass at fixed richness. The X-ray luminosity at fixed optical richness is distributed in a lognormal manner with mean

$$\bar{\ell}(\nu) \ = \ p(\bar{\mu}(\nu) + \alpha\, r\, \sigma_{\mu|\nu}\sigma_{\mu|\ell}), \tag{4}$$

and variance

$$\sigma^2_{\ell|\nu} \ = \ p^2\left(\sigma^2_{\mu|\nu} + \sigma^2_{\mu|\ell} - 2r\sigma_{\mu|\nu}\sigma_{\mu|\ell}\right), \tag{5}$$

where p is the slope of the halo $L_X - M_{200}$ relation.

When L_X and N_{200} are independent ($r = 0$), the mean luminosity reflects that of the mean mass selected by the richness cut. When $r \neq 0$, the mean is shifted by an amount that scales linearly with the mass function slope α. If the scatter is constant, then this shift affects all N_{200}-binned points equally, and the slope of the richness-binned $L_X - M_{200}$ relation will be unbiased, $\mathrm{d}\bar{\ell}(\nu)/\mathrm{d}\bar{\mu}(\nu) = p$. However, in cold dark matter models, the slope α runs with mass, and this running can induce a change in slope at the level $\Delta p/p = r\sigma_{\mu|\nu}\sigma_{\mu|\ell}[\mathrm{d}\alpha(\mu)/\mathrm{d}\mu]$.

The inset in Fig. 1 explicitly demonstrates this effect for the case $p = 1.6, \sigma_{\mu|\ell} = 0.25$ and $\sigma_{\mu|\nu} = 0.5$. We use a discrete set of haloes from the Hubble Volume simulation (Evrard et al. 2002) that define a mass function which is not a power law (Jenkins et al. 2001). To each halo, we assign richness and luminosity using a constant lognormal covariance, and then bin the sample on optical richness and compute mean luminosities and masses for each bin. Imposing a correlation coefficient $r = \pm 0.7$ tilts the richness-binned L_X–M_{200} slope by ∼0.2, or roughly 1.5σ, given the error in equation (3).

As discussed in Nord et al. (2008), covariance can both tilt the scaling relation and modify the scatter. The second observable quantity affected by r is the variance in L_X at fixed richness N_{200} (equation 5). This scatter was constrained in R08 to be $\sigma_{\ell|\nu} = 0.86 \pm 0.03$. In our model, it takes on values of 1.1, 0.90 and 0.72 for $r = -0.7$, 0 and 0.7, respectively. We stress that these values are sensitive to the assumed degree of mass scatter at fixed N_{200}. Our assumed value of 0.5 is smaller than that inferred by the spread in galaxy velocity dispersions at fixed richness (Becker et al. 2007) and employed by Johnston et al. (2007) in the lensing analysis. Using this larger

scatter would result in $\sigma_{\ell|\nu} > 1$ for all $r \in [-1, 1]$. If the R08 measurement of $\sigma_{\ell|\nu} \lesssim 0.9$ is correct, then either the Becker et al. (2007) scatter is an overestimate or the simple lognormal model employed here is insufficient.

Improved understanding of the variance is clearly desired. Constraints on $\sigma_{\ell|\nu}$ can be obtained by individual X-ray follow-up observations of richness-selected maxBCG subsamples. Such data can also generate hydrostatic mass estimates, enabling constraints on the mass scatter $\sigma_{\mu|\nu}$. Such a study would begin to test all the elements of the full covariance $P(\ell, \nu|\mu)$ used to describe the underlying massive halo population.

5 SUMMARY

In this Letter, we present a new measurement of the scaling between X-ray luminosity and mass using ∼17 000 optically selected clusters of galaxies. X-ray luminosities are derived from RASS photon maps, while masses are determined independently through modelling of the mean cluster lensing profiles. Binning clusters by optical richness, we find that the mean L_X and M_{200} values follow a power-law relation with slope 1.65 ± 0.13. The consistency in slope with previous studies, including those based on hydrostatic mass estimates, confirms that the optically selected maxBCG catalogue selects a population of massive haloes similar to those of X-ray samples. The consistency implies that systematic errors in hydrostatic mass are not strongly scale-dependent. Furthermore, we demonstrate how the slope can be affected by covariance in L_X and N_{200} at a fixed mass, and show that this covariance is not large.

Follow-up X-ray observations of N_{200} selected subsamples would provide key information on the covariance, as expressed in equation (5). Data from future deep surveys, selected via optical, X-ray and Sunyaev–Zel'dovich signatures, will provide a much richer environment for addressing the complex interplay between cosmology and covariant scaling relations.

ACKNOWLEDGMENTS

ESR and TAMcK are pleased to acknowledge financial support from NSF AST-0206277 and AST-0407061, and the hospitality of the MCTP. ESR also thanks the TABASGO foundation. AEE acknowledges support from NSF AST-0708150. We thank A. Finoguenov, T. Reiprich and H. Boehringer for helpful feedback.

REFERENCES

Bardeau S., Soucail G., Kneib J.-P., Czoske O., Ebeling H., Hudelot P., Smail I., Smith G. P., 2007, A&A, 470, 449
Becker M. R. et al., 2007, ApJ, 669, 905
Böhringer H. et al., 2004, A&A, 425, 367
Ebeling H., Voges W., Bohringer H., Edge A. C., Huchra J. P., Briel U. G., 1996, MNRAS, 281, 799
Evrard A. E., 1990, ApJ, 363, 349
Evrard A. E. et al., 2002, ApJ, 573, 7
Finoguenov A., Reiprich T. H., Böhringer H., 2001, A&A, 368, 749
Gioia I. M., Maccacaro T., Schild R. E., Wolter A., Stocke J. T., Morris S. L., Henry J. P., 1990, ApJS, 72, 567
Hansen S. M., McKay T. A., Wechsler R. H., Annis J., Sheldon E. S., Kimball A., 2005, ApJ, 633, 122
Hoekstra H., 2007, MNRAS, 379, 317
Jenkins A., Frenk C. S., White S. D. M., Colberg J. M., Cole S., Evrard A. E., Couchman H. M. P., Yoshida N., 2001, MNRAS, 321, 372
Johnston D. E. et al., 2007, preprint (arXiv:0709.1159)
Koester B. P. et al., 2007a, ApJ, 660, 221
Koester B. P. et al., 2007b, ApJ, 660, 239
Mantz A., Allen S. W., Ebeling H., Rapetti D., 2007, MNRAS, submitted (arXiv:0709.4294)
Nagai D., Vikhlinin A., Kravtsov A. V., 2007, ApJ, 655, 98
Navarro J. F., Frenk C. S., White S. D. M., 1997, ApJ, 490, 493
Nord B., Stanek R., Rasia E., Evrard A. E., 2008, MNRAS, 383, L10
Rasia E., Mazzotta P., Borgani S., Moscardini L., Dolag K., Tormen G., Diaferio A., Murante G., 2005, ApJ, 618, L1
Reiprich T. H., Böhringer H., 2002, ApJ, 567, 716
Rosati P., Borgani S., Norman C., 2002, ARA&A, 40, 539
Rozo E. et al., 2007, preprint (astro-ph/0703571)
Rykoff E. S. et al., 2008, ApJ, 675, 1106
Sheldon E. S. et al., 2007, preprint (arXiv:0709.1153)
Stanek R., Evrard A. E., Böhringer H., Schuecker P., Nord B., 2006, ApJ, 648, 956
Vikhlinin A., Kravtsov A., Forman W., Jones C., Markevitch M., Murray S. S., Van Speybroeck L., 2006, ApJ, 640, 691
Voges W. et al., 1999, A&A, 349, 389
Voit G. M., 2005, Rev. Mod. Phys., 77, 207
Wechsler R. H., Zentner A. R., Bullock J. S., Kravtsov A. V., Allgood B., 2006, ApJ, 652, 71
York D. G. et al., 2000, AJ, 120, 1579

This paper has been typeset from a TEX/LATEX file prepared by the author.